Journal of Experimental Marine Biology and Ecology 593 (2025) 152146

Contents lists available at ScienceDirect

Journal of Experimental Marine Biology and Ecology

journal homepage: www.elsevier.com/locate/jembe

Sargassum leachate initially inhibits then stimulates phytoplankton growth in coral reef waters

Pascal Claquin [a,*], Isabelle Mussio [a], Maxime Navon [a], Anne-Marie Rusig [a], Amélia Chatagnon [b,c], Charlotte Dromard [b,c]

[a] UR 7482 MERSEA - Marine Ecosystems and oRganisms reSEArch Lab - Université de Caen Normandie, CREC - Station Marine - BP49, 54, rue du Docteur Charcot, 14530 Luc-sur-Mer, France
[b] Laboratoire Biologie des ORganismes et Ecosystèmes Aquatiques (BOREA), UMR 8067, Muséum National d'Histoire Naturelle, Sorbonne Université, CNRS, IRD-207, Université des Antilles, France
[c] Laboratoire d'Excellence « CORAIL », Université des Antilles, Campus de Fouillole, 97157 Pointe-à-Pitre, Guadeloupe, France

ARTICLE INFO

Keywords:
Phytoplankton
Sargassum leachate
Photosynthesis
Allelopathy
Controlled conditions

ABSTRACT

Massive *Sargassum* accumulations in the Atlantic form the Great Atlantic *Sargassum* Belt, which fuels recurrent coastal inundation events that disrupt ecosystems by reducing light availability for phytoplankton and enriching nearshore waters with nutrients released during decomposition. This study examined the short-term effects of decaying *Sargassum* leachate on phytoplankton productivity and growth in Guadeloupe's coral reef ecosystems using several photosynthesis measurements based on fluorescence and ^{13}C. A range of leachate concentrations were applied, under controlled conditions, to a natural phytoplankton community. The study revealed two major effects of *Sargassum* leachate on phytoplankton. First, leachate at concentrations ≥1 % initially inhibited photosynthesis and growth up to Day 2, likely due to allelopathic substances such as polyphenols. This was evidenced by near-zero Fv/Fm values and disrupted electron transport in PSII. By Day 3, these inhibitory effects diminished, suggesting degradation of labile inhibitory compounds or community modification. Second, from Day 3 onward, leachate addition stimulated phytoplankton growth, as seen in increased biomass, primary production (JVIImax), and carbon fixation. This nutrient-driven response was accompanied by reduced C/Chl a ratios and improved photosynthetic efficiency (lower Φe,C values), indicating alleviation of nutrient limitations, particularly nitrogen and phosphorus. These findings underscore the dual role of *Sargassum* leachate: an initial suppressive impact through allelopathy and a subsequent nutrient enrichment effect driving phytoplankton blooms. Such dynamics highlight the significant and complex influence of *Sargassum* strandings, combining ecological stress with nutrient-driven productivity changes.

1. Introduction

Over the past decade, massive accumulations of holopelagic *Sargassum* spp., including *S. natans* (morphotypes I and VIII) and *S. fluitans* (morphotype III), have been observed in the equatorial Atlantic Ocean (Siuda et al., 2024). These aggregations constitute the Great Atlantic Sargassum Belt, which periodically drives large-scale inundation and stranding events along the coasts of the West Indies, Brazil, and West Africa (Berline et al., 2020; García-Sánchez et al., 2020; Gower et al., 2013; Schell et al., 2015; Wang et al., 2019). While floating *Sargassum* supports diverse marine communities (Alleyne et al., 2023a; Alleyne et al., 2023b; Sissini et al., 2017; van Tussenbroek et al., 2024a), stranded or inundated *Sargassum* can negatively impact benthic and pelagic organisms, coral larvae, food webs, (Antonio-Martínez et al., 2020; Cabanillas-Terán et al., 2019; Theirlynck et al., 2023; van Tussenbroek et al., 2024b) and primary producers, particularly phytoplankton. Dense *Sargassum* mats reduce light penetration, which inhibits photosynthesis and limits phytoplankton productivity (van Tussenbroek et al., 2017). Additionally, decomposing stranded *Sargassum* releases ammonium, organic matter, and toxic leachate containing arsenic and heavy metals, further degrading water quality and altering nutrient cycles in coastal waters (Devault et al., 2021; Morelle and Claquin, 2018; Napoleon and Claquin, 2012; Olguin-Maciel et al., 2022; Rodríguez-Martínez et al., 2019; Rodríguez-Martínez et al., 2025; van Tussenbroek

* Corresponding author.
E-mail address: pascal.claquin@unicaen.fr (P. Claquin).

https://doi.org/10.1016/j.jembe.2025.152146
Received 23 June 2025; Received in revised form 30 September 2025; Accepted 4 November 2025
Available online 8 November 2025

et al., 2017).This nutrient influx, particularly dissolved inorganic nitrogen (DIN) and phosphorus (DIP), disrupts the oligotrophic conditions typical of tropical marine ecosystems, where nitrogen often limits algal growth (Andrews and Gentien, 1982; Kleypas et al., 1999; Patey et al., 2008; Raikar and Wafar, 2006). Decaying *Sargassum* enriches the surrounding water with nitrogen and phosphorus, fueling phytoplankton blooms and favoring fast-growing opportunistic species over perennial ones (Hanisak, 1993; Lapointe et al., 2021; van Tussenbroek et al., 2017). Such shifts can destabilize local algal communities and contribute to broader ecosystem changes, including competition with corals (Arias-González et al., 2017).

The aim of our study was to assess the impacts of decaying *Sargassum* on phytoplankton within the coral reef ecosystems of Guadeloupe Island (French Antilles). To this end, we exposed a natural phytoplankton community, collected from a Sargassum-free zone, to a gradient of environmentally realistic leachate concentrations. Previous research has already highlighted the negative effects of Sargassum leachates on water quality and on the behavior of coral larvae in the Caribbean (Antonio-Martínez et al., 2020), as well as the capacity of *Sargassum* species, both fresh and dried, to inhibit phytoplankton growth and photosynthesis (Wang et al., 2007; Zhang et al., 2021). Building on these findings, we specifically aimed to evaluate effects of leachates from decaying *Sargassum* on phytoplankton, combining photosynthetic performance measurements obtained with a Single Turnover Active Fluorometer (LabSTAF) (Boatman et al., 2019; Schuback et al., 2021) and ^{13}C isotopic uptake analyses (Morelle and Claquin, 2018; Napoleon and Claquin, 2012). The LabSTAF employs seven excitation wavebands centered at 416, 452, 473, 495, 534, 594, and 622 nm, which can be combined to target a range of photosynthetic pigments based on their spectral characteristics (Courtecuisse et al., 2023). This approach allowed us to generate photosynthesis–irradiance curves (Fluorescent Light Curves – FLCs) and estimate key photosynthetic parameters, such as the maximal electron transport rate of PSII (ETR_{IImax}) and model primary production (Serre-Fredj et al., 2023). By coupling electron transport rate measurements with ^{13}C isotopic incorporation, we estimated the electron requirement for carbon fixation (Φe,C), a parameter that responds to nutrient availability (Hughes et al., 2018; Lawrenz et al., 2013; Napoleon and Claquin, 2012; Zhu et al., 2016) and taxonomic composition (Hughes et al., 2021; Napoleon et al., 2013) and allow to convert ETR to carbon photosynthetic flux. The main objective of this experiment was to assess the short-term impact (few days) of *Sargassum* leachate on phytoplankton growth and productivity. A range of leachate concentrations were applied, under controlled conditions, to a natural phytoplankton community sampled in Guadeloupe from a *Sargassum* free zone. Biomass growth (*Chl*a) and several photosynthetic parameters (variable fluorescence and ^{13}C) have been monitored during seven days.

Our study contributes to a better understanding of the impact of decaying *Sargassum* on the planktonic compartment of Caribbean ecosystems by highlighting the physiological and ecological effects of *Sargassum* leachate on a natural phytoplankton community.

2. Materials & methods

2.1. Enrichment experiment

2.1.1. Production and characterization of Sargassum leachate

In October 2021, five kilograms of frozen *Sargassum* biomass collected in July 2020 were thawed and soaked for 48 h in stagnant seawater under a shaded outdoor structure. The collected *Sargassum* was a mixture of three morphotypes (*S. fluitans* III, *S. natans* I, and *S. natans* VIII), commonly found in massive strandings of holopelagic *Sargassum* along the Caribbean coast (Siuda et al., 2024). The biomass was then removed using coarse and sequential filtration processes, followed by sterilization of the leachate through Millipore filtration (0.22 μm). The sterile leachate was analysed for nutrient concentrations, including dissolved inorganic nitrogen (DIN) and phosphate ($PO4^{3-}$), dissolved organic carbon (DOC) and dissolved organic nitrogen (DON). The nutrient composition of the leachate was 15.17 μM NO_3^-, 0.588 μM NO_2^-, 406.72 μM NH_4^+ and 410 μM PO_4^{3-} with the ratio NID/ PO_4^3 close to 1. The DOC and DON concentrations were respectively 112.60 mM C and 3.43 mM N.

2.1.2. Seawater sampling and leachate addition

Eighty liters of seawater were collected in four polypropylene round carboys of 20 L at a one-meter depth, in the "Grand cul de sac Marin", in a *Sargassum* free zone (Supplementary Fig. 1). The carboys were placed in the dark in a cooler to maintain temperature and were immediately brought back to the laboratory. Initial measurements corresponding to T0 for all parameters monitored were common to all conditions. The seawater was homongenized to prevent settling and then immediately distributed randomly into ventilated 1 L polycarbonate flasks containing 600 ml of sample. Leachate additions were made at five concentrations ranging from 0 to 1 % (vol/vol) in triplicates corresponding to a series of 15 flasks per sampling day (Treatment A: 0 %; Treatment B: 0.01 %; Treatment C: 0.1 %; Treatment D: 0.5 %; Treatment E: 1 %). In this way, all samples were independent of each other during time monitoring. For example, the 15 flasks sampled on Day 7 were not sampled on the previous days. Incubations were carried during seven days under controlled conditions at 29 °C (as seawater temperature at this season) under 311 μmol photon.m^{-2}.s^{-1} provide by LED sources Optonica H150-A2 150W, 6000 k with a 12 h/12 h L/D photoperiod (The light spectrum is shown in Supplementary Fig. 2).

2.2. Incubation parameters and nutrient analyses

Water temperature and light intensity were recorded throughout the experiment with an RBRsolo T logger and a RBR solo PAR logger connected to a Li-COR LI-192. Nutrient concentrations were recorded and analysed at regular interval during the experiment. For the analyses of inorganic nutrients, a sample of water was collected from each condition and filtered through a cellulose acetate filter (ClearLine, CA, 33 mm, 0.45 μm) in 50 mL Falcon tubes and frozen (−20 °C). Analyses were conducted using a Seal Analytical AA3 system (Aminot and Kerouel, 2007). The limits of quantification were 0.02 μmol L^{-1} for PO_4^{3-} and 0.05 μmol L^{-1} for NO_3^-. NH_4^+ were analysed by fluorometric measurements (Holmes et al., 1999). Measurements of dissolved organic carbon (DOC) and total nitrogen (TN) in the leachate were carried out using TOC-L-CSH with a unit of TNM (Shimadzu) following the protocol proposed by Halewood et al. (2022).

At Day 0, the concentrations of treatments B, C, D, and E were derived from the initial concentration of treatment A, adjusted according to the proportion of leachate added.

2.3. Chl a biomass

For each sample, 250 mL were filtered through a polycarbonate filter (Millipore, 47 mm, 0.2 μm) and immediately frozen (−20 °C) prior to analysis. Aliquots (10 mL of 90 % acetone, *v*/v) were added for pigment extraction then the samples were left for 12 h in the dark at 4 °C. After being centrifuged for 5 min at 1700*g* twice, the Chl *a* concentration of the extracts was measured using a Trilogy fluorimeter (Turner Designs, Sunnyvale, USA) (Strickland and Parsons, 1972).

2.4. Photosynthetic parameters

In order to assess phytoplankton primary production and photosynthetic parameters an approach based on a single-turnover variable chlorophyll fluorescence method was used during the experiments. This non-invasive method base on biophysical occurring in the photosystem II (PSII) is fast and robust to estimate primary production (Boatman et al., 2019; Courtecuisse et al., 2023; Schuback et al., 2021; Serre-Fredj et al., 2023). Fluorescent light curves (FLCs) were performed using a

LabSTAF (Chealsea Technology, UK) (Oxborough, 2022). The samples were analysed after a 3-min period of dark incubation for oxidation of quinone A (Q_A). A single turnover (ST) saturation phase was delivered with a 100-μs solid excitation pulse (450 nm). Primary fluorescence surper acquisition (Saq) values, relaxation phase parameters and derived fluorescence parameters are derived using the Rho ST curve fit based on the equations proposed by (Kolber et al., 1998) which is completed by the Dimer ST curve fit (see Oxborough, 2022 for details). From theses fits the minimum (F_o) and maximum fluorescence (F_m) are notably estimated, as described in Boatman et al. (2019) and detailed in Oxborough (2022). The maximum quantum efficiency of PSII (F_v/F_m) was calculated as Genty et al. (1989) (Eq. 1):

$$\frac{F_v}{F_m} = \frac{(F_m - F_o)}{F_m} \quad (1)$$

Samples were then exposed to 10 light steps of increasing PAR (from 0 to 2000 μmol photon. $s^{-1}.m^{-2}$) for 30-s each step. The effective quantum efficiency of PSII ($F_{q'}/F_{m'}$) was measured at each light step as (Genty et al., 1989) (Eq. 2):

$$\frac{F_{q'}}{F_{m'}} = \frac{(F_{m'} - F')}{F_{m'}} \quad (2)$$

where $F_{m'}$ is the maximum fluorescence under light and F' is the steady state fluorescence under light.

The relative electron transport rate (rETR, relative unit) was calculated for each irradiance (E) as (Eq. 3):

$$rETR(E) = \frac{F_{q'}}{F_{m'}} \times E \quad (3)$$

The maximum relative electron transport rate ($rETR_{max}$) was estimated by fitting the FLC data to the model of Webb et al. (1974) modified by Boatman et al. (2019) using RunSTAF (Chelsea Technologies, UK) software to estimate α and E_k with α, the initial slope of the FLC, and E_k the light saturation index (Eq. 4):

$$rETR(E) = \alpha \times E_K \times \left(1 - e^{\frac{-E}{E_K}}\right) - \beta \times E_{K\beta} \times \left(1 - e^{\frac{-E-E_K}{E_{K\beta}}}\right) \quad (4)$$

$rETR_{max}$ was calculated as:

$$rETR_{max} = \alpha \times E_K \quad (5)$$

Relative values of electron flux (rETR) represent an intermediate step in the calculation; however, only the absolute values described below were considered in the results presented.

Using the absorption algorithm of Oxborough et al. (2012), the absorption coefficient for PSII light harvesting was calculated as follows:

$$a_{LHII} = \frac{F_m \times F_o}{F_m - F_o} \times K_a \times 10^{-6} \quad (6)$$

where K_a is an inherent constant of the LabSTAF. The absolute PSII electron flux per unit volume ($JVP_{II(E)}$) which account for the phytoplankton production was calculated as:

$$JVP_{II(E)} = \frac{a_{LHII} \times rETR_{(E)} \times 3600}{10^3} \quad (7)$$

where $JVP_{II(E)}$ is expressed in mmol $e^-.m^{-3}.h^{-1}$. (See Supplementary Fig. 3 for an exemple).

The absolute electron transport rate ($ETR_{II(E)}$) at each light intensity which account for the phytoplankton productivity (e.g. production by units of biomass) was calculated as:

$$ETR_{II(E)} = \frac{JV_{IIII(E)max}}{[chl\ a]} \quad (8)$$

where [chl *a*] is the concentration of chl *a* ($\mu g.L^{-1}$). The $ETR_{II(E)}$ is expressed in in mmol e^-.mg $chla^{-1}.h^{-1}$.

By applying $rETR_{max}$ to eq. 7, JVP_{IImax} was calculated. Then, by applying JVP_{IImax} to eq. 8, ETR_{IImax} was calculated.

It is important to mention that a high correlation was determined between F_o and [chl *a*] for all tested conditions and the following relationship was established: [chl *a*] = 1.089 F_o ($r^2 = 0.95$; $p < 0.001$).

2.5. Fluorescence spectral analysis

The LabSTAF (Chelsea Technologies, UK) enables the performance of photochemical excitation profiles (PEP) (Courtecuisse et al., 2023). In the LabSTAF, fluorescence transients are induced using Measurement LEDs (MLEDs) at seven distinct wavelengths (416, 452, 473, 495, 534, 595, and 622 nm), providing access to Fv and σ_{PII} (functional absorption cross-section) for each wavelength. As described by Gorbunov et al. (2020), PEP can be utilized for both physiological and taxonomic analyses of phytoplankton communities based on secondary photosynthetic pigments. Indeed, major functional groups of phytoplankton primarily differ and are characterized by their pigment composition. In this study, Fv(λ) and σ_{PII} (λ)were used to identify changes in community structures as a function of treatments. To eliminate the effects of changes in fluorescence intensity due to variations in biomass and to emphasize changes in spectral shape, reflecting community composition and/or alterations in pigments, the normalization procedure proposed by Alexander et al. (2012) was applied on Fv data. Fv spectra were normalized by dividing the value for each measurement wavelength by the average value across the seven measurement wavelengths.

2.6. ^{13}C incubation

^{13}C incubation experiments were conducted at T0 just afer sampling and before leachate additions and at day 5 on the triplicate of all tested conditions. For each ^{13}C incubation, a 62 mL sub-sample was inoculated with $NaH^{13}CO_3$ (98 atom %, Sigma-Aldrich) corresponding to an enrichment of about 50 % of the dissolved inorganic carbon already present. The inoculated ^{13}C flasks were placed at the same condition that incubated samples, i.e. 29 °C under 311 μmol photon.$m^{-2}.s^{-1}$. For each condition one flask was maintained in the dark to estimate non-photosynthetic inorganic carbon incorporation. After 3.5 h of incubation, each flask was filtered onto 25 mm pre-combusted (450 °C, 12 h) GF/F filters and stored at 20 °C until analysis. To remove carbonates, filters were exposed to fuming HCl for four hours and then dried at 50 °C for 12 h. The concentration of particulate organic carbon (POC) and the isotopic ratio of ^{13}C to ^{12}C were determined using an EA 3000 elemental analyzer (Eurovector, Milan, Italy) combined with a mass spectrophotometer (IsoPrime, Elementar). The value for incorporation in the dark was subtracted from all data. The carbon fixation rate (P^B) was calculated according to Hama et al. (1983) and expressed in mmol C mg Chl a^{-1} h^{-1} as decribed in Napoleon and Claquin (2012).

2.7. Statistical analysis

Shapiro Wilk's Test and Bartlett's test were used to examine the data normality and their homogeneity of variance, respectively. The results were used to categorize parametric and non-parametric data. To evaluate changes Kruskal-Wallis and Wilcox's post hoc were used for non-parametric data, while ANOVA and post-hoc Tukey tests were carried out for parametric data.

Analyse of Fv and σ_{PII} spectra: To highlight the effects of treatments, time, and their interactions on the shape of the spectra, PERMANOVA (Permutational Multivariate Analysis of Variance) based on Euclidean distances and 999 permutations was performed, followed by post hoc ADONIS (Analysis of Dissimilarities) pairwise analyses (Martinez Arbizu, 2020). PCoA (Principal Coordinates Analysis) was used to represent PERMANOVA results based on Euclidean distances. This approach highlights multivariate patterns by projecting the data into a lower-dimensional space, facilitating visualization of group separations.

The consistency of the Euclidean distance metric ensures coherence between statistical testing and graphical representation. R studio and the following package were used, vegan and pairwiseAdonis (Martinez Arbizu, 2020).

3. Results

The chlorophyll *a* (Chl *a*) concentration in the control group (A) exhibited a modest increase during the incubation period, rising from 0.16 µgChla L^{-1} at T0 to a peak of 0.65 µgChla L^{-1} at Day 5, followed by a decrease to 0.46 at Day 7 (Fig. 1a). Introduction of leachate at B, C, and D concentrations resulted in a substantial augmentation of biomass, with a rapid growth observed at Day 4, followed by a slight decline. Interestingly, condition E demonstrated a distinctive pattern, wherein the biomass remained lower during the first 2 days, then gradually increased to 0.22 µgChla L^{-1} at Day 3. Subsequently, the concentration rose to 3.27 at Day 4 and peaked at 16.81 at Day 5, before decreasing marginally (Fig. 1). The biomass levels observed on Day 7 correspond to the increasing leachate inputs from A to E.

Nutrient concentrations exhibited marked temporal dynamics across treatments with increasing proportions of *Sargassum* leachate (Fig. 2). At Day 0, concentrations in treatments B to E were calculated based on the initial concentration in treatment A, according to the percentage of leachate added (A: 0 %; B: 0.01 %; C: 0.1 %; D: 0.5 %; E: 1.0 %). Ammonium (NH_4^+) showed the most pronounced variations: treatments D and E, and C to a lesser extent, displayed sharp increases during the first days, whereas treatment A remained near baseline (Fig. 2a). The maximum mean value of 18.71 µM was reached in treatment E at Day 2, after which NH_4^+ concentrations declined to an average of 1.2 µM by Day 6 in treatments D and E. Phosphate (PO_4^{3-}) concentrations showed drop occurred between T0 and T1 in treatments C, D and E, with concentrations decreasing by factors of 2.1, 3.0 and 3.5, respectively (Fig. 2b). Nitrate (NO_3^-) decreased over time, although an increase was observed in treatment E at Day 6 (Fig. 2c). Nitrite (NO_2^-) concentrations remained low throughout the experiment and showed no consistent trends (Fig. 2d). Overall, these results indicate that *Sargassum* leachate is a significant source of dissolved inorganic nitrogen and phosphorus, with effects that scale with leachate concentration.

The Fv/Fm ratio exhibited a consistent decline across all incubation conditions throughout the experiment, decreasing from 0.48 at T0 to an average of 0.34 by Day 7 (Fig. 1b). Treatment E displayed a distinctive pattern once again. The ST curve fittings (Rho ST curve fit and Dimer ST curve fit) applied to raw fluorescence super acquisition (Saq) data obtained in the dark from the first ST pulse were not able to converge to the data, and the estimation of Fv/Fm was therefore not possible from Day 1 to Day 2. (Supplementary Fig. 4). The measurements can be considered as noise and do not reflect any clear photosynthetic activity. For this reason, zero values were plotted in the graphs to indicate the inability of the models to fit the data.

Notably, on Day 3, aligning with the observed growth in Chl *a* biomass measurements, the Fv/Fm ratio rebounded in treatment E. It is noteworthy that for leachate additions exceeding 1 % (and 2 %, 5 % data not shown), the phytoplankton community also displayed near-zero Fv/Fm values after just one day.

The ETR_{IImax} (Fig. 1c), representing the maximal photosynthetic capacity of the phytoplankton community in the samples, exhibited an

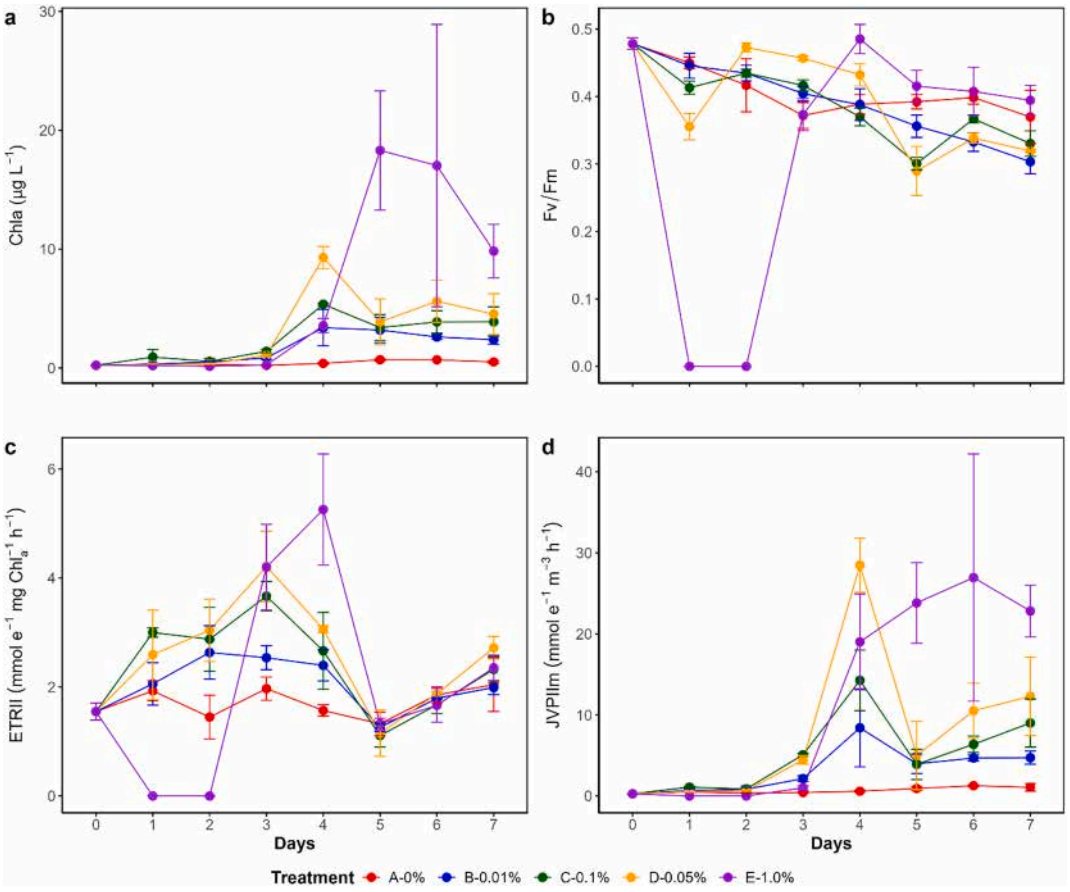

Fig. 1. **a**-Dynamics of chlorophyll *a* concentration (in µg L^{-1}) for the different treatments applied as a function of time. **b**,**c**,**d** Labstaf measurements for the different treatments as a function of time: **a** - Dynamics of maximal quatum yield of PSII (Fv/Fm). **b**- Dynamics of the absolute electron transport rate of PSII (ETR_{IImax}) expressed in in mmol e^-.mg $chla^{-1}.h^{-1}$. **c**- Dynamics of the PSII electron flux per unit volume (JVP_{IImax}) which account for the phytoplankton production expressed in mmol $e^-.m^{-3}.h^{-1}$.

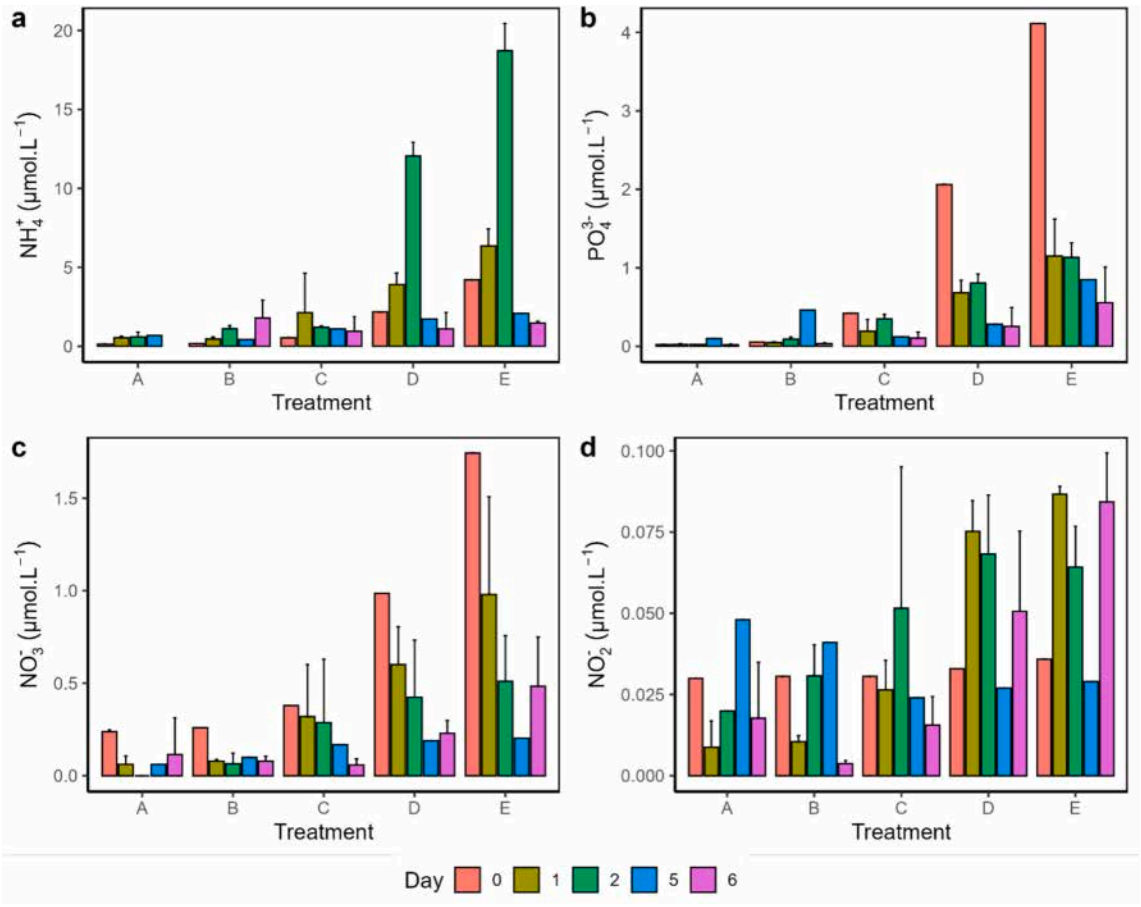

Fig. 2. Concentration of nutrients as a function of the time. **a**- NH_4^+ in µmol L^{-1}. **b**- PO_4^{3-} in µmol L^{-1}. **c**- NO_3^- in µmol L^{-1}. **c**- NO_2^- in µmol L^{-1}. At Day 0, the concentrations of treatments B, C, D, and E were derived from the initial concentration of treatment A, adjusted according to the proportion of leachate added (A: 0 %; B: 0.01 %; C: 0.1 %; D: 0.5 %; E: 1.0 %). The NH_4^+ concentration of treatment A at Day 6 was not available, and only one flask was sampled per treatment at Day 5.

upward trend in response to leachate concentrations during the initial two days in treatments A to D, while a decline to null values in treatment E was observed. By Day 3, the ETR in treatment E rebounded, reaching a peak on Day 4. At Day 7, the ETR_{IImax} levels across all treatments were comparable, showing minimal variation without significant differences (Fig. 1c).

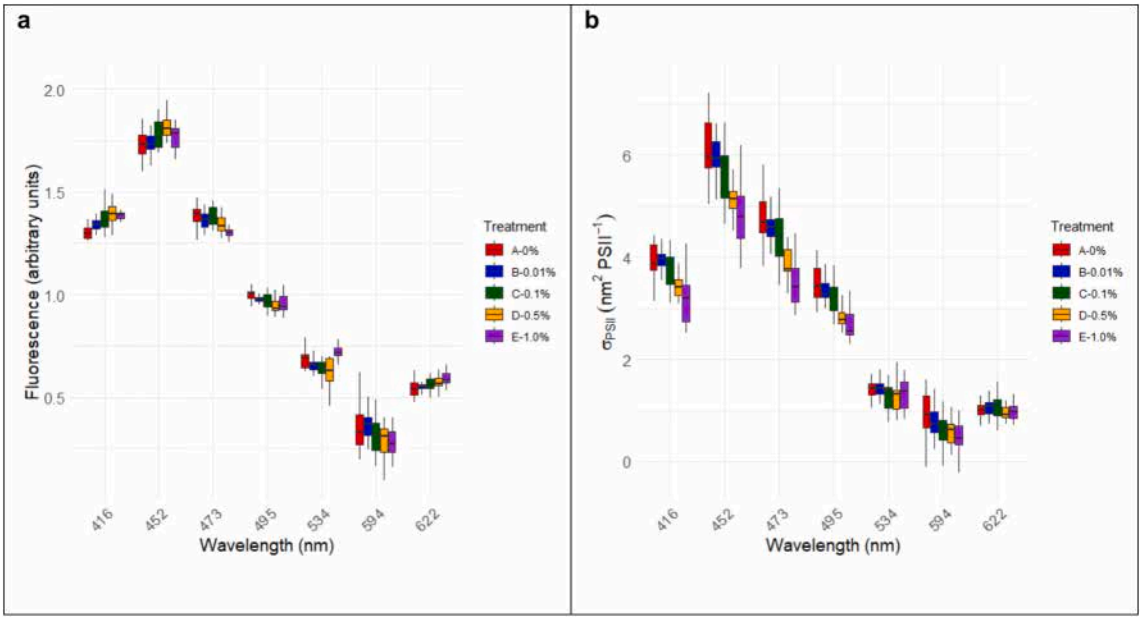

Fig. 3. Spectral of Fv (**a**) and Sigma (**b**) for the different treatments applied.

JVIImax (Fig. 1d), representing maximal primary production in terms of electrons generated per m^3 per hour, is an outcome derived from the interplay of productivity (ETR_{IImax}) and biomass. Given the relatively consistent dynamics of ETR_{II} across various treatments (except for the distinctive behavior in treatment E), the patterns observed in primary production align closely with those of biomass. By the seventh day, the leachate addition gradient comes to the forefront once more, showcasing an increase in production from treatments A to E, characterized by mean values expressed in mmol electrons m^{-3} h^{-1} of 1.07 for A, 4.73 for B, 9.01 for C, 12.30 for D and 22.82 for E.

The Fv(λ) and $\sigma_{PII}(\lambda)$ spectra, which provide insights into changes in community structures (Fig. 3), exhibited a globally similar shape across all treatments. However, PERMANOVA and PCOA analyses revealed significant differences between treatments (Fig. 4, Table 1) and over time (data not shown) for both the Fv(λ) and $\sigma_{PII}(\lambda)$ spectra. While conditions A and B showed no significant differences for either spectrum type, all other conditions differed significantly from A, except for condition C in the case of the $\sigma_{PII}(\lambda)$ spectrum. Conditions C and D were comparable for these parameters, but condition E displayed significant differences from all other conditions for both spectra, except for condition D in the case of the $\sigma_{PII}(\lambda)$ spectrum.

It was observed that as the concentration of leachate increased, the POC levels also rose, in accordance with the concomitant increase in Chl *a* biomass. On Day 5, the POC concentrations exhibited significant variations across all tested treatments (ANOVA $P = 0.001$, Holm-Sidak; $p < 0.05$) (Fig. 5A), except for the comparisons between A and B treatments and between C and D treatments.

A significant decrease in the C/Chl *a* ratio was observed between the control (A) and the treatments with added leachate. The ratio exhibited a large variation, with a fivefold decrease from 316 to 62 (mean values). Interestingly, no significant differences were identified among the B, C, and D treatments (Fig. 5B), all of which displayed values around 150.

On Day 5, we assessed photosynthetic production (Fig. 6a) and productivity (Fig. 6b) through ^{13}C incorporation. The addition of leachate resulted in an augmentation of production, particularly noteworthy in Treatment E, evident from the elevated and statistically significant values also observed in JVIImax, another indicator of photosynthetic production capacity. The productivity, indicative of photosynthetic activity under incubation light intensity (Fig. 6b), exhibited a significant increase in Treatments C and E compared to A, while showing no statistically significant difference from Treatments B and D. Consequently, the introduction of leachate contributed to an enhancement in photosynthetic activity.

Labstaf data allow us to determine the electron product at the PSII incubation light intensity (absolute electron transport rate, ETRII) in parallel with ^{13}C fixation on day 5 (Fig. 7). Integrating these measurements allows us to estimate the moles of electrons needed to fix one mole of carbon (Φe,C). The results reveal that the introduction of leachate leads to a significant reduction in the Φe,C value, suggesting enhanced efficiency in electron transport within the photosynthetic chain. The average value of Φe,C with leachate addition was 5.24 mol electron mol C^{-1}, while it was 12.23 mol electron mol C^{-1} for Treatment A (without leachate addition).

4. Discussion

This study provides new insights into the short-term impacts of *Sargassum* leachates on natural phytoplankton communities. Monitoring of both biomass and photosynthetic parameters revealed contrasting responses, highlighting the dual role of *Sargassum* leachates as both potential stressors and nutrient sources for phytoplankton. The results showed an initial inhibition of photosynthesis and growth at concentrations equal to or above 1 % during the first two days, followed by a subsequent stimulation of phytoplankton growth from the third day onward.

The selection of leachate concentrations was guided by Rodríguez-Martínez et al. (2019), who reported mean ammonium concentrations of approximately 6 μM (ranging from 4.6 to 8.8 μM) between 45 and 450 m from the shore following *Sargassum* strandings. The experimental design was therefore established to remain within this order of magnitude for the highest concentrations. As previously reported, *Sargassum* decomposition increases both ammonium and phosphate concentrations (Rodríguez-Martínez et al., 2019; Rodríguez-Muñoz et al., 2021). The rise in ammonium observed in treatments C, D, and E likely reflects remineralization of the labile fraction of dissolved organic nitrogen (DON), which was abundant in the leachate (3.43 mM N), a process

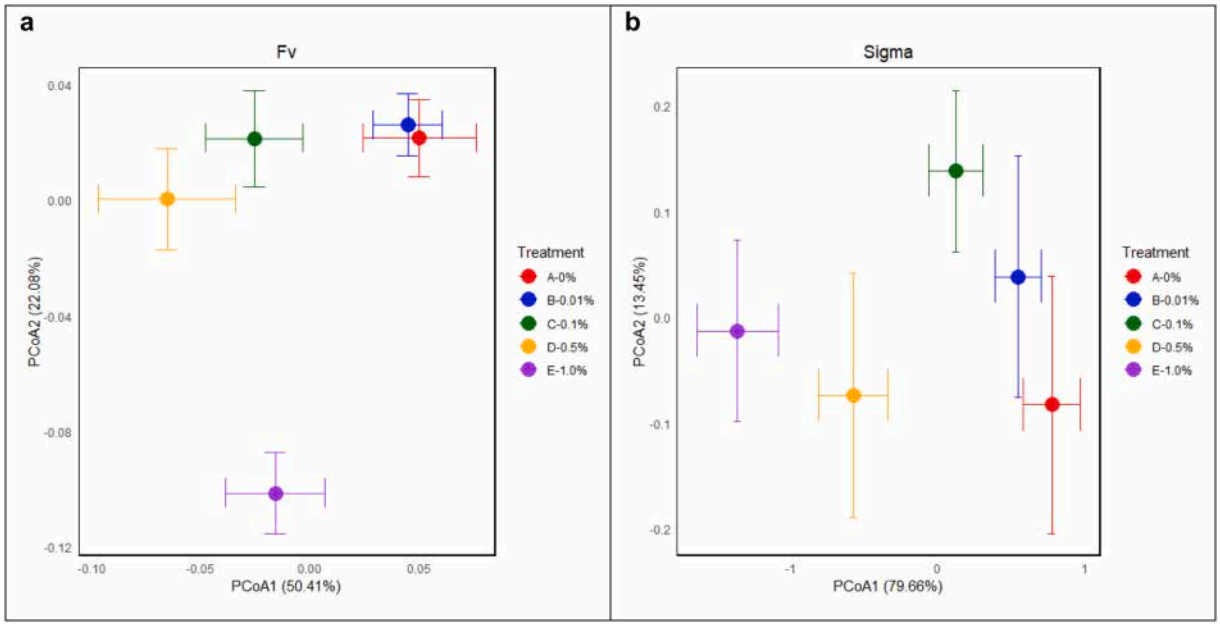

Fig. 4. Spectral variations of Fv (**a**) and Sigma (**b**) for the different treatments applied depicted by PCoA plot of weighted Euclidien distances. PERMANOVA, $p < 0.001$ for Treatment factor for both spectra. Centroids for each sampling time are shown along with their standard errors (error bars). ADONIS Fv, R2 = 0.21 $p = 0.001$; ADONIS Sigma; $R^2 = 0.32$ $p = 0.001$.

Table 1
: Results of the post hoc ANODIS pairwise analyses of PERMAVOVA. The "p.adjusted" value is the *p*-value adjusted to account for the issue of multiple comparisons. If the adjusted p-value is less than 0.05, it indicates that the difference between the groups remains significant even after correction for multiple comparisons. The significant differences between the treatments are highlighted in gray.

Treatments	Fv spectrum				Sigma spectrum			
Pairs	F.Model	R^2	p.value	p.adjusted	F.Model	R^2	p.value	p.adjusted
A vs B	2.58	0.06	0.059	0.59	0.99	0.02	0.378	1
A vs C	5.33	0.11	0.002	0.02	4.72	0.10	0.025	0.25
A vs D	10.99	0.20	0.001	0.01	13.93	0.24	0.001	0.01
A vs E	10.50	0.22	0.001	0.01	30.46	0.45	0.001	0.01
B vs C	3.29	0.08	0.02	0.2	2.24	0.05	0.103	1
B vs D	7.70	0.16	0.001	0.01	10.98	0.22	0.001	0.01
B vs E	13.01	0.28	0.001	0.01	29.71	0.47	0.001	0.01
C vs D	2.16	0.05	0.076	0.76	4.58	0.10	0.023	0.23
C vs E	7.34	0.18	0.001	0.01	17.72	0.34	0.002	0.02
D vs E	4.67	0.12	0.003	0.03	3.94	0.10	0.033	0.33

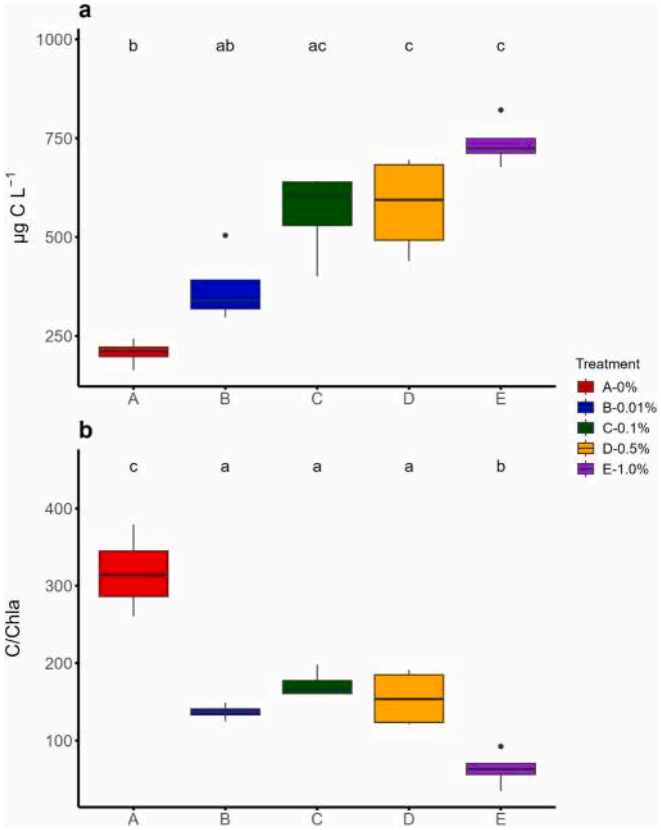

Fig. 5. **a** - Particulate Organic Carbone (POC) expressed in µg $C^{-}.L^{-1}$ at day 5 for the different treatments applied. Groups a, b, c pointed out by ANOVA (P = 0.001, TukeyHSD<0.05). **b** - Carbon/Chlorophyll ratio at day 5 for the different treatments applied. Groups a, b, c pointed out by Kruskal-Wallis test (H = 15.829 with 4 degrees of freedom (P = 0.003), Tukey<0.05).

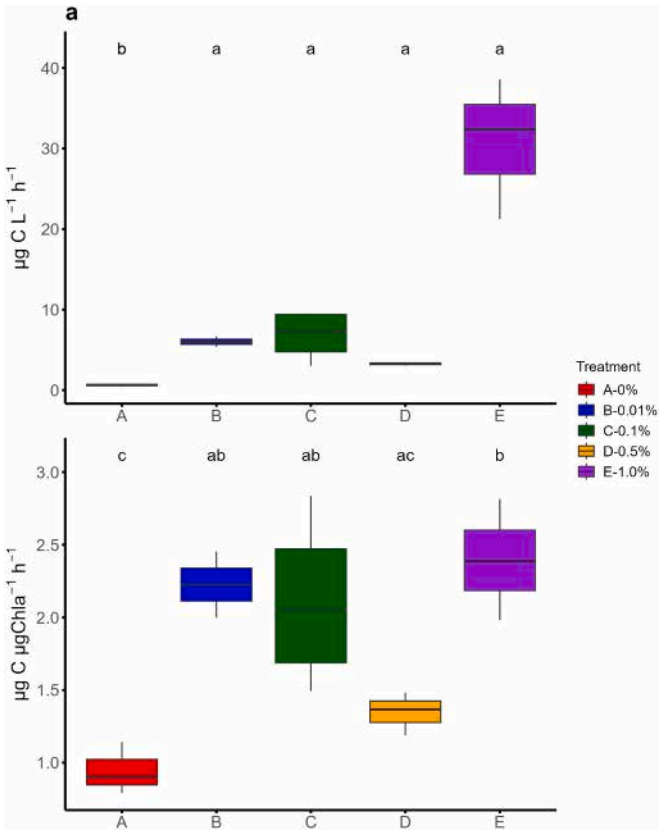

Fig. 6. **a** - Production of carbon per litre, at growth light intensity, measured by using ^{13}C incubation, expressed in µg $C.L^{-1}.h^{-1}$ at day 5 for the different treatments. Groups a, b pointed out by Kruskal-Wallis test (H = 11.70 with 4 degrees of freedom (P = 0.02), Tukey<0.05). **b**- Production of carbon per biomass unit, at growth light intensity, measured by using ^{13}C incubation, expressed in µg $C.µg\ chla^{-1}.h^{-1}$ at day 5 for the different treatments applied. Groups a, b, c pointed out by ANOVA (P = 0.006, Holm-Sidak<0.05).

largely mediated by heterotrophic bacteria consistent with the trends observed in the present experiment. The activity of heterotrophic bacteria may also explain the observed decrease in phosphate concentrations in these treatments, despite the absence of phytoplankton growth and even the inhibition of photosynthesis in treatment E. Indeed, heterotrophic bacteria are often strong competitors for inorganic phosphorus (including orthophosphate) and can outcompete phytoplankton in oligotrophic waters (Duhamel, 2025; Michelou et al., 2011; Popendorf and Duhamel, 2015). A complementary biogeochemical study, including a detailed investigation of microbial loop functioning, would therefore be valuable to refine the present observations on nutrient dynamics.

Although elevated ammonium concentrations can be toxic to phytoplankton (Berg et al., 2017; Collos and Harrison, 2014),

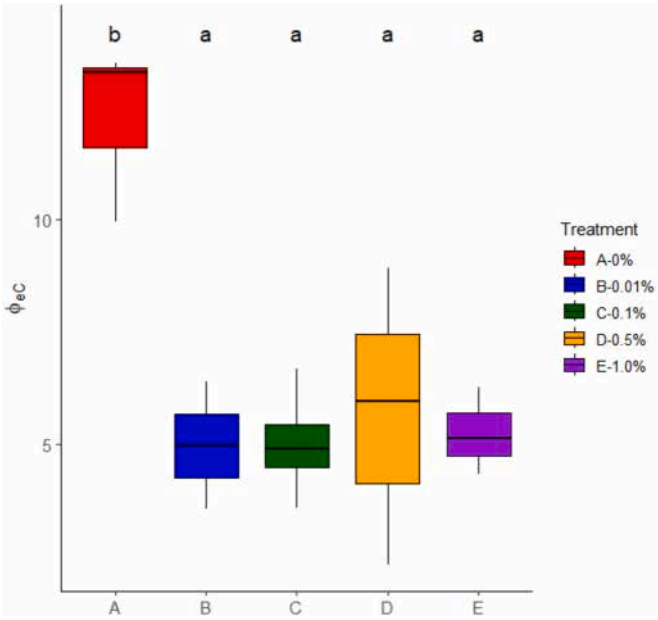

Fig. 7. Electron requirement (mol electron required to fix one mol of carbon) for the different treatments applied. Groups a, b pointed out by ANOVA ($P = 0.005$, Holm-Sidak<0.05).

concentrations below 100 μM, as in the present study, are unlikely to reduce the growth rate of most microalgae (Keller et al., 1987) or to affect Fv/Fm (Berg et al., 2017). The sudden increase in ammonium concentration observed in treatment E therefore does not appear sufficient on its own to explain the transient inhibition of photosynthesis and growth, although a partial contribution cannot be entirely excluded.

This points to the involvement of additional inhibitory compounds released during *Sargassum* decomposition. Indeed, the inhibition observed with a 1 % leachate addition is consistent with previous studies reporting allelopathic effects of macroalgal substances or tissues on phytoplankton (Belleza et al., 2019; Havens et al., 2001; Tang and Gobler, 2011; Wang et al., 2012; Wang et al., 2009). Wang et al. (2007) showed that fresh tissue, dry powder and aqueous extracts of *Sargassum thunbergii* strongly inhibited the growth of the microalgae *Heterosigma akashiwo* (Raphidophyceae) and *Alexandrium tamarense* (Dinophyceae) as we observed in the present study. Such a result was also found by Zhang et al. (2021) with another species of *Sargassum, S. fusiforme*. They showed that *Sargassum* extract inhibited growth, led to a decrease of the maximal quantum yield (Fv/Fm) and affect Chl *a* cell content on the three tested microalgae (*Prorocentrum donghaiensis*, *Skeletonema costatum, and Heterosigma akashiwo*). Sun et al. (2021) also highlighted the allelopathic effects of *S. fusiforme* on *H. akashiwo*, demonstrating that α-linolenic acid (ALA) and 24-hydroperoxy-24-vinylcholesterol strongly inhibited algal growth. They further showed that ALA disrupted antioxidant activity and reduced the photosynthetic PSII electron transport rate.

A negative allelopathic effect of *Sargassum* on *Ulva prolifera* photosynthesis has also been demonstrated, affecting processes ranging from the quantum efficiency of PSII to RUBISCO activity (Sun et al., 2024). revealed that *Sargassum* filtrate negatively impacts the photosynthesis of *Ulva* by damaging cellular membranes, particularly chloroplasts, and reducing starch granule numbers (Sun et al., 2024). This damage decreases photosynthetic efficiency, alters enzyme activities, and triggers oxidative stress. Rubisco activity, essential for carbon fixation, was inhibited, leading to metabolic adjustments, including increased starch hydrolysis and upregulation of the pentose phosphate pathway to maintain photosynthesis under stress. In the present work, since ST curve fitting was not possible after 24 h for the highest concentration (Treatment E), Fv/Fm can be assumed to be negligible, and the electron transport rate through PSII was substantially inhibited by 1 % leachate, ultimately leading to growth inhibition. As mentioned by Zhang et al. (2021), the inhibitory substances in the extracts are presumably secondary metabolism which alter PSII. Polyphenols is wildy mentioned as an allelochemicals produced by macroalgae. Flavonoids, natural polyphenols, which are largely present in *Sargassum* (Afreen et al., 2023; Paredes-Camacho et al., 2023) were reported to inactivate algae chlorophyll (Li et al., 2022) as we observed in the present study. The inactivation processus are still unclear, but it can be due to the loss of Mg^{2+} ions from Chl *a* (Li et al., 2022).

On the third day, at the concentration of 1 % addition, we observed a rebound in photosynthetic parameters and growth. The result was confirmed across all replicates, which it is important to note, were independent even between the follow-up days. Two hypotheses can be proposed to explain this result:

Hypothesis 1. The leachate has a lethal effect on the community, and only a small proportion survives, eventually taking over the initial community and blooming on the third day.

Hypothesis 2. The leachate inhibits photosynthesis and growth through labile substances that could be rapidly degradable, losing their inhibitory effectiveness after 2 days.

Spectral fluorescence relies on the excitation-emission characteristics of phytoplankton taxa, which are influenced by their accessory pigments (Beutler et al., 2002; Chen et al., 2017; Harrison et al., 2016; MacIntyre et al., 2010; Seppala and Balode, 1997). Each group exhibits distinct fluorescence excitation patterns based on pigments such as Chl *a*, Chl *c*, phycocyanobilin, phycoerythrobilin, fucoxanthin, and peridinin. These patterns enable the differentiation of phytoplankton spectral groups, including Chlorophyta, Cyanobacteria, "chromophyta" (Heterokontophyta, Haptophyta, Dinophyta), and Cryptophyta. Gorbunov et al. (2020) demonstrated that $\sigma_{PII}(\lambda)$ spectrum can be used to characterize phytoplankton spectral groups, as they found that intra-group variability of $\sigma_{PII}(\lambda)$ spectrum was significantly lower than inter-group differences. In the present study, we analysed variations in the overall spectral shape, following the approach of Alexander et al. (2012), to assess changes in community structure. However, we did not attempt to identify specific phytoplankton spectral groups. Our data revealed a consistent overall shape of $Fv(\lambda)$ and $\sigma_{PII}(\lambda)$ spectra across all treatments over the seven-day period, suggesting only minor changes in phytoplankton spectral composition (Beutler et al., 2002; Gorbunov et al., 2020). However, significant differences were observed between treatments. Treatment E exhibited significant deviations from all other conditions for both spectra, except for condition D in the case of the $\sigma_{PII}(\lambda)$ spectrum. The slight but significant variations observed are likely attributable to physiological effects induced by enrichment from the leachate rather than shifts in community composition (Gorbunov et al., 2020; Suggett et al., 2009). This finding supports the hypothesis that leachate composition inhibits photosynthesis and growth rather than selecting for a resistant phytoplankton community. Our results demonstrate a severe effect of leachate on growth and photosynthesis, indicating that *Sargassum* strandings can have significant and rapid effects on the pelagic compartment. Many studies have shown that growth-inhibiting allelophatic substances degrade rapidly, and the inhibitory effect can be maintained by supplying the allelochemicals regularly (Havens et al., 2001; Wang et al., 2007; Wang et al., 2009). However, we cannot exclude a variation in the community within phytoplankton spectral groups. An analysis of molecular diversity would allow us to go further in understanding this effect. Indeed, it was also show that allelochemicals inhibitory effects varied with species and growing densities of the microalgae leading to community variation (Zhang et al., 2021).

The second effect highlighted is directly related to the nutrient enrichment provided by the leachate. We observe that from day 3, biomass and JVIImax increase in correlation with the enrichment level, then stabilize before slightly decreasing on Day 6. The obtained curves

are characteristic of a "bloom" growth pattern with an exponential phase followed by a plateau indicating a Liebig-type limitation (Dolman and Wiedner, 2015). Thus, the addition of leachate has alleviated a nutrient limitation. Nutrient analyses we conducted, considering the very low concentrations naturally present in the environment, do not allow us to conclude whether leachate addition lifted a limitation in N or in P. On Day 5, the highest concentration of particulate organic carbon (POC) and carbon production was linked to the increased leachate input. The range of the C/Chl *a* ratio measured during the study was in accordance with values observed on oligothrophic phytoplankton communities (Ortiz et al., 2022). We observed that the addition of leachate was correlated with a reduction in the C/Chl *a* ratio, which can be attributed to the growth rate increase. The Φe,C values were in accordance with literature (Hughes et al., 2021; Lawrenz et al., 2013; Morelle and Claquin, 2018), and the low values measured on Day 5 following leachate addition confirm the influence of nutrient input on photosynthetic efficiency. The decrease in Φe,C observed between Treatment A compared to other treatments is indicative of a nutrient-replete condition (Napoleon et al., 2013). Under nutrient limitation, alternative electron pathways, including the Mehler reaction and cyclic electron flow around PSI, result in an elevation of Φe,C values (Hughes et al., 2021; Lawrenz et al., 2013; Morelle and Claquin, 2018; Napoleon et al., 2013).

5. Conclusion

Our study revealed two distinct effects of *Sargassum* leachate on phytoplankton. 1) the addition of leachate led to a pronounced inhibition of photosynthesis and growth, particularly at concentrations equal to or greater than 1 %. This inhibitory impact, observed up to Day 2, was characterized by the inhibition of electron transport through PSII. The possible effect of polyphenols, such as flavonoids, in the leachate as to be more deeply explored. Our findings underscore the severe and rapid impact of *Sargassum* strandings on the pelagic compartment, suggesting that allelopathic substances may play a role on phytoplankton communities. 2) our study highlighted a positive impact on phytoplankton growth from day 3 onwards. The correlation between leachate addition and increased particulate organic carbon (POC) concentration, ETR_{II}, carbon production, and reduced C/Chla ratio suggested a nutrient-driven response. Our findings also showed the influence of nutrient input on photosynthetic regulation, as reflected the impact on Φe,C values.

Taken together, these contrasting responses illustrate the complex interplay between allelopathic effects and nutrient enrichment in the context of Sargassum leachates. While phytoplankton growth was stimulated in controlled laboratory conditions, such responses are unlikely to fully translate to natural environments at large scale, where nutrient dilution in the water column and reduced light penetration under *Sargassum* mats or during decomposition events may mask or attenuate any positive nutrient effects. This study therefore contributes valuable insights into the ecological consequences of *Sargassum* strandings on Caribbean ecosystems, highlighting the need to consider both stressor and nutrient enrichment effects when assessing their overall impact.

CRediT authorship contribution statement

Pascal Claquin: Writing – review & editing, Writing – original draft, Validation, Methodology, Investigation, Formal analysis, Data curation, Conceptualization. **Isabelle Mussio:** Writing – review & editing, Writing – original draft, Investigation, Funding acquisition, Conceptualization. **Maxime Navon:** Writing – review & editing, Investigation, Conceptualization. **Anne-Marie Rusig:** Writing – review & editing, Investigation, Conceptualization. **Amélia Chatagnon:** Writing – review & editing, Investigation. **Charlotte Dromard:** Writing – review & editing, Investigation, Funding acquisition, Conceptualization.

Declaration of competing interest

The authors declare that they have no known competing financial interests or personal relationships that could have appeared to influence the work reported in this paper.

Acknowledgment

This study was funded by the ARN SAVE-C from the SARGASSUM Joint Call, "Research, Development and Innovation". We thank S. Cordonnier from the University of the Antilles and O. Jolly and C. Massinot from the University of Caen Normandy for their technical assistance. We are most grateful to the platform PLATIN from the US EMERODE of the University of Caen Normandy for ^{13}C and carbon pools analysis used in this study.

Appendix A. Supplementary data

Supplementary data to this article can be found online at https://doi.org/10.1016/j.jembe.2025.152146.

Data availability

Data will be made available on request.

References

Afreen, A.B., Rasool, F., Fatima, M., 2023. Bioactive properties of brown seaweed, *Sargassum wightii* and its nutritional, therapeutic potential and health benefits: a review. J. Environ. Biol. 44, 146–158.
Alexander, R., Gikuma-Njuru, P., Imberger, J., 2012. Identifying spatial structure in phytoplankton communities using multi-wavelength fluorescence spectral data and principal component analysis. Limnol. Oceanogr. 10, 402–415.
Alleyne, K.S.T., Johnson, D., Neat, F., Oxenford, H.A., Vallès, H., 2023a. Seasonal variation in morphotype composition of pelagic *Sargassum* influx events is linked to oceanic origin. Sci. Rep. 13.
Alleyne, K.S.T., Small, M., Corbin, M., Valles, H., Oxenford, H.A., 2023b. Free-swimming fauna associated with influxes of pelagic sargassum: implications for management and harvesting. Front. Mar. Sci. 10.
Aminot, A., Kerouel, R., 2007. Dosage automatique des nutriments dans les eaux marines. Ifremer-Quae, Versailles.
Andrews, J.C., Gentien, P., 1982. Upwelling as a source of nutrients for the great barrier-reef ecosystems - a solution to Darwin question. Mar. Ecol. Prog. Ser. 8, 257–269.
Antonio-Martínez, F., Henaut, Y., Vega-Zepeda, A., Ceron-Flores, A.I., Raigoza-Figueras, R., Cetz-Navarro, N.P., Espinoza-Avalos, J., 2020. Leachate effects of pelagic *Sargassum* spp. on larval swimming behavior of the coral *Acropora palmata*. Sci. Rep. 10, 3912.
Arias-González, J.E., Fung, T., Seymour, R.M., Garza-Pérez, J.R., Acosta-González, G., Bozec, Y.M., Johnson, C.R., 2017. A coral-algal phase shift in Mesoamerica not driven by changes in herbivorous fish abundance. PloS One 12, e0174855.
Belleza, D.F.C., Wagas, E.C., Aaron, J.L.J., Abao, R.S.A., Dy, D.T., 2019. Allelopathic effects of three intertidal marine macrophytes on the growth of *Nanochlorum* sp. J. Environ. Sci. Manag. 22, 13–19.
Berg, G.M., Driscoll, S., Hayashi, K., Ross, M., Kudela, R., 2017. Variation in growth rate, carbon assimilation, and photosynthetic efficiency in response to nitrogen source and concentration in phytoplankton isolated from upper San Francisco Bay. J. Phycol. 53, 664–679.
Berline, L., Ody, A., Jouanno, J., Chevalier, C., André, J.M., Thibaut, T., Ménard, F., 2020. Hindcasting the 2017 dispersal of *Sargassum* algae in the Tropical North Atlantic. Mar. Pollut. Bull. 158, 111431.
Beutler, M., Wiltshire, K.H., Meyer, B., Moldaenke, C., Lüring, C., Meyerhöfer, M., Hansen, U.P., Dau, H., 2002. A fluorometric method for the differentiation of algal populations *in vivo* and *in situ*. Photosynth. Res. 72, 39–53.
Boatman, T.G., Geider, R.J., Oxborough, K., 2019. Improving the accuracy of single turnover active fluorometry (STAF) for the estimation of phytoplankton primary productivity (PhytoPP). Front. Mar. Sci. 6, 319.
Cabanillas-Terán, N., Hernández-Arana, H.A., Ruiz-Zárate, M.A., Vega-Zepeda, A., Sanchez-Gonzalez, A., 2019. *Sargassum* blooms in the Caribbean alter the trophic structure of the sea urchin *Diadema antillarum*. Peerj 7, e7589.
Chen, P., Pan, D.L., Wang, T.Y., Mao, Z.H., Zhang, Y.W., 2017. Coastal and inland water monitoring using a portable hyperspectral laser fluorometer. Mar. Pollut. Bull. 119, 153–161.
Collos, Y., Harrison, P.J., 2014. Acclimation and toxicity of high ammonium concentrations to unicellular algae. Mar. Pollut. Bull. 80, 8–23.
Courtecuisse, E., Marchetti, E., Oxborough, K., Hunter, P.D., Spyrakos, E., Tilstone, G.H., Simis, S.G.H., 2023. Optimising multispectral active fluorescence to distinguish the photosynthetic variability of cyanobacteria and algae. Sensors 23, 461.

Devault, D.A., Pierre, R., Marfaing, H., Dolique, F., Lopez, P.J., 2021. *Sargassum* contamination and consequences for downstream uses: a review. J. Appl. Phycol. 33, 567–602.
Dolman, A.M., Wiedner, C., 2015. Predicting phytoplankton biomass and estimating critical N:P ratios with piecewise models that conform to Liebig's law of the minimum. Freshw. Biol. 60, 686–697.
Duhamel, S., 2025. The microbial phosphorus cycle in aquatic ecosystems. Nat. Rev. Microbiol. 23, 239–255.
García-Sánchez, M., Graham, C., Vera, E., Escalante-Mancera, E., Alvarez-Filip, L., van Tussenbroek, B.I., 2020. Temporal changes in the composition and biomass of beached pelagic *Sargassum* species in the Mexican Caribbean. Aquat. Bot. 167, 103275.
Genty, B., Briantais, J.M., Baker, N.R., 1989. The relationship between the quantum yield of photosynthetic electron-transport and quenching of chlorophyll fluorescence. Biochim. Biophys. Acta 990, 87–92.
Gorbunov, M.Y., Shirsin, E., Nikonova, E., Fadeev, V.V., Falkowski, P.G., 2020. A multi-spectral fluorescence induction and relaxation (FIRe) technique for physiological and taxonomic analysis of phytoplankton communities. Mar. Ecol. Prog. Ser. 644, 1–13.
Gower, J., Young, E., King, S., 2013. Satellite images suggest a new *Sargassum* source region in 2011. Remote Sens. Lett. 4, 764–773.
Halewood, E., Opalk, K., Custals, L., Carey, M., Hansell, D.A., Carlson, C.A., 2022. Determination of dissolved organic carbon and total dissolved nitrogen in seawater using high temperature combustion analysis. Front. Mar. Sci. 9.
Hama, T., Miyazaki, T., Ogawa, Y., Iwakuma, T., Takahashi, M., Otsuki, A., Ichimura, S., 1983. Measurement of photosynthetic production of a marine-phytoplankton population using a stable C-13 isotope. Mar. Biol. 73, 31–36.
Hanisak, M.D., 1993. Nitrogen release from decomposing seaweeds - species and temperature effects. J. Appl. Phycol. 5, 175–181.
Harrison, J.W., Howell, E.T., Watson, S.B., Smith, R.E.H., 2016. Improved estimates of phytoplankton community composition based on *in situ* spectral fluorescence: use of ordination and field-derived norm spectra for the bbe FluoroProbe. Can. J. Fish. Aquat. Sci. 73, 1472–1482.
Havens, K.E., Hauxwell, J., Tyler, A.C., Thomas, S., McGlathery, K.J., Cebrian, J., Valiela, I., Steinman, A.D., Hwang, S.J., 2001. Complex interactions between autotrophs in shallow marine and freshwater ecosystems: implications for community responses to nutrient stress. Environ. Pollut. 113, 95–107.
Holmes, R.M., Aminot, A., Kérouel, R., Hooker, B.A., Peterson, B.J., 1999. A simple and precise method for measuring ammonium in marine and freshwater ecosystems. Can. J. Fish. Aquat. Sci. 56, 1801–1808.
Hughes, D.J., Campbell, D.A., Doblin, M.A., Kromkamp, J.C., Lawrenz, E., Moore, C.M., Oxborough, K., Prásil, O., Ralph, P.J., Alvarez, M.F., Suggett, D.J., 2018. Roadmaps and detours: active chlorophyll-*a* assessments of primary productivity across marine and freshwater systems. Environ. Sci. Technol. 52, 12039–12054.
Hughes, D.J., Giannini, F.C., Ciotti, A.M., Doblin, M.A., Ralph, P.J., Varkey, D., Verma, A., Suggett, D.J., 2021. Taxonomic variability in the electron requirement for carbon fixation across marine phytoplankton. J. Phycol. 57, 111–127.
Keller, M.D., Selvin, R.C., Claus, W., Guillard, R.R.L., 1987. Media for the culture of oceanic ultraphytoplankton. J. Phycol. 23, 633–638.
Kleypas, J.A., McManus, J.W., Meñez, L.A.B., 1999. Environmental limits to coral reef development: where do we draw the line? Am. Zool. 39, 146–159.
Kolber, Z.S., Prásil, O., Falkowski, P.G., 1998. Measurements of variable chlorophyll fluorescence using fast repetition rate techniques:: defining methodology and experimental protocols. Biochimica Et Biophysica Acta-Bioenergetics 1367, 88–106.
Lapointe, B.E., Brewton, R.A., Herren, L.W., Wang, M., Hu, C., McGillicuddy, D.J., Lindell, S., Hernandez, F.J., Morton, P.L., 2021. Nutrient content and stoichiometry of pelagic *Sargassum* reflects increasing nitrogen availability in the Atlantic Basin. Nat. Commun. 12.
Lawrenz, E., Silsbe, G., Capuzzo, E., Ylöstalo, P., Forster, R.M., Simis, S.G.H., Prásil, O., Kromkamp, J.C., Hickman, A.E., Moore, C.M., Forget, M.H., Geider, R.J., Suggett, D. J., 2013. Predicting the electron requirement for carbon fixation in seas and oceans. PloS One 8.
Li, J., Yao, Y.R., Hu, X., Wang, J., Yin, L., Zhang, Y., Ni, L.X., Li, S.Y., Zhu, F.X., 2022. Inactivation mechanism of algal chlorophyll by allelochemical quercetin. Bull. Environ. Contam. Toxicol. 109, 450–458.
MacIntyre, H.L., Lawrenz, E., Richardson, T.L., 2010. Taxonomic discrimination of phytoplankton by spectral fluorescence. In: Suggett, D., Prášil, O., Borowitzka, M. (Eds.), Chlorophyll a Fluorescence in Aquatic Sciences: Methods and Applications, Developments in Applied Phycology, 4. Springer, Dordrecht, pp. 281–304.
Martinez Arbizu, P., 2020. PairwiseAdonis: Pairwise Multilevel Comparison Using Adonis (R. Package Version 0.4). https://github.com/pmartinezarbizu/pairwiseAdonis.
Michelou, V.K., Lomas, M.W., Kirchman, D.L., 2011. Phosphate and adenosine-5′-triphosphate uptake by cyanobacteria and heterotrophic bacteria in the Sargasso Sea. Limnol. Oceanogr. 56, 323–332.
Morelle, J., Claquin, P., 2018. Electron requirements for carbon incorporation along a diel light cycle in three marine diatom species. Photosynth. Res. 137, 201–214.
Napoleon, C., Claquin, P., 2012. Multi-parametric relationships between PAM measurements and carbon incorporation, an *in situ* approach. PloS One 7, e40284.
Napoleon, C., Raimbault, V., Claquin, P., 2013. Influence of nutrient stress on the relationships between PAM measurements and carbon incorporation in four phytoplankton species. PloS One 8, e66423.
Olguin-Maciel, E., Leal-Bautista, R.M., Alzate-Gaviria, L., Domínguez-Maldonado, J., Tapia-Tussell, R., 2022. Environmental impact of *Sargassum* spp. landings: an evaluation of leachate released from natural decomposition at Mexican Caribbean coast. Environ. Sci. Pollut. Res. 29, 91071–91080.
Ortiz, J., Arístegui, J., Hernández-Hernández, N., Fernández-Méndez, M., Riebesell, U., 2022. Oligotrophic phytoplankton community effectively adjusts to artificial upwelling regardless of intensity, but differently among upwelling modes. Front. Mar. Sci. 9.
Oxborough, K., 2022. LabSTAF and RunSTAF Handbook: 2408–014-HB. Issue F. Chelsea Technologies Ltd, West Molesey, UK.
Oxborough, K., Moore, C.M., Suggett, D.J., Lawson, T., Chan, H.G., Geider, R.J., 2012. Direct estimation of functional PSII reaction center concentration and PSII electron flux on a volume basis: a new approach to the analysis of Fast Repetition Rate fluorometry (FRRf) data. Limnol. Oceanogr. 10, 142–154.
Paredes-Camacho, R.M., González-Morales, S., González-Fuentes, J.A., Rodríguez-Jasso, R.M., Benavides-Mendoza, A., Charles-Rodríguez, A.V., Robledo-Olivo, A., 2023. Characterization of *Sargassum* spp. from the Mexican Caribbean and its valorization through fermentation process. Processes 11, 685.
Patey, M.D., Rijkenberg, M.J.A., Statham, P.J., Stinchcombe, M.C., Achterberg, E.P., Mowlem, M., 2008. Determination of nitrate and phosphate in seawater at nanomolar concentrations. Trends Anal. Chem. 27, 169–182.
Popendorf, K.J., Duhamel, S., 2015. Variable phosphorus uptake rates and allocation across microbial groups in the oligotrophic Gulf of Mexico. Environ. Microbiol. 17, 3992–4006.
Raikar, V., Wafar, M., 2006. Surge ammonium uptake in macroalgae from a coral atoll. J. Exp. Mar. Biol. Ecol. 339, 236–240.
Rodríguez-Martínez, R.E., Medina-Valmaseda, A.E., Blanchon, P., Monroy-Velázquez, L. V., Almazán-Becerril, A., Delgado-Pech, B., Vásquez-Yeomans, L., Francisco, V., García-Rivas, M.C., 2019. Faunal mortality associated with massive beaching and decomposition of pelagic *Sargassum*. Mar. Pollut. Bull. 146, 201–205.
Rodríguez-Martínez, R.E., Torres-Conde, E.G., Rosellón-Druker, J., Cabanillas-Terán, N., Jáuregui-Haza, U., 2025. The Great Atlantic Sargassum Belt: impacts on the central and Western Caribbean-a review. Harmful Algae 144, 102838.
Rodríguez-Muñoz, R., Muñiz-Castillo, A.I., Euán-Avila, J.I., Hernández-Núñez, H., Valdés-Lozano, D.S., Collí-Dulá, R.C., Arias-González, J.E., 2021. Assessing temporal dynamics on pelagic *Sargassum* influx and its relationship with water quality parameters in the Mexican Caribbean. Reg. Stud. Mar. Sci. 48, 102005.
Schell, J.M., Goodwin, D.S., Siuda, A.N.S., 2015. Recent *Sargassum* inundation events in the Caribbean: Shipboard observations reveal dominance of a previously rare form. Oceanography 28, 8–10.
Schuback, N., Tortell, P.D.D., Berman-Frank, I., Campbell, D.A.A., Ciotti, A., Courtecuisse, E., Erickson, Z.K.K., Fujiki, T., Halsey, K., Hickman, A.E.E., Huot, Y., Gorbunov, M.Y.Y., Hughes, D.J.J., Kolber, Z.S.S., Moore, C.M., Oxborough, K., Prásil, O., Robinson, C.M.M., Ryan-Keogh, T.J.J., Silsbe, G., Simis, S., Suggett, D.J.J., Thomalla, S., Varkey, D.R.R., 2021. Single-turnover variable chlorophyll fluorescence as a tool for assessing phytoplankton photosynthesis and primary productivity: opportunities, caveats and recommendations. Front. Mar. Sci. 8, 690607.
Seppala, J., Balode, M., 1997. The use of spectral fluorescence methods to detect changes in the phytoplankton community. Hydrobiologia 363, 207–217.
Serre-Fredj, L., Chasselin, L., Jolly, O., Claquin, P., 2023. Complex drivers of primary production along an anthropised estuary (Seine estuary-France). Front. Environ. Sci. 11, 1216732..
Sissini, M.N., Barreto, M., Széchy, M.T.M., de Lucena, M.B., Oliveira, M.C., Gower, J., Liu, G., Bastos, E.D., Milstein, D., Gusmao, F., Martinelli, J.E., Alves-Lima, C., Colepicolo, P., Ameka, G., de Graft-Johnson, K., Gouvea, L., Torrano-Silva, B., Nauer, F., Nunes, J.M.D., Barufi, J.B., Rörig, L., Riosmena-Rodríguez, R., Mello, T.J., Lotufo, L.V.C., Horta, P.A., 2017. The floating *Sargassum* (Phaeophyceae) of the South Atlantic Ocean - likely scenarios. Phycologia 56, 321–328.
Siuda, A.N.S., Blanfuné, A., Dibner, S., Verlaque, M., Boudouresque, C.F., Connan, S., Goodwin, D.S., Stiger-Pouvreau, V., Viard, F., Rousseau, F., Michotey, V., Schell, J. M., Changeaux, T., Aurelle, D., Thibaut, T., 2024. Morphological and molecular characters differentiate common morphotypes of atlantic holopelagic *Sargassum*. Phycology 4, 256–275.
Strickland, J.D.H., Parsons, T.R., 1972. A Practical Hand Book of Seawater Analysis, second/Ed. Fisheries Research Board of Canada Bulletin.
Suggett, D.J., Moore, C.M., Hickman, A.E., Geider, R.J., 2009. Interpretation of fast repetition rate (FRR) fluorescence: signatures of phytoplankton community structure versus physiological state. Mar. Ecol. Prog. Ser. 376, 1–19.
Sun, S., Hu, S., Zhang, B., Sun, X., Xu, N., 2021. Allelopathic effects and potential allelochemical of *Sargassum fusiforme* on red tide microalgae *Heterosigma akashiwo*. Mar. Pollut. Bull. 170, 112673.
Sun, R.B., Korboon, O., Ma, W.F., Ren, X.Y., Wang, X.N., Muangmai, N., Xing, Q.K., Gao, X., Li, J.Y., 2024. Allelopathic interactions between the green-tide-forming *Ulva prolifera* and the golden-tide-forming *Sargassum horneri* under controlled laboratory conditions. Plants 13, 2966.
Tang, Y.Z., Gobler, C.J., 2011. The green macroalga, *Ulva lactuca*, inhibits the growth of seven common harmful algal bloom species via allelopathy. Harmful Algae 10, 480–488.
Theirlynck, T., Mendonça, I.R.W., Engelen, A.H., Bolhuis, H., Collado-Vides, L., van Tussenbroek, B.I., García-Sánchez, M., Zettler, E., Muyzer, G., Amaral-Zettler, L., 2023. Diversity of the holopelagic *Sargassum* microbiome from the Great Atlantic *Sargassum* Belt to coastal stranding locations. Harmful Algae 122, 102369.
van Tussenbroek, B.I., Arana, H.A.H., Rodríguez-Martínez, R.E., Espinoza-Avalos, J., Canizales-Flores, H.M., González-Godoy, C.E., Barba-Santos, M.G., Vega-Zepeda, A., Collado-Vides, L., 2017. Severe impacts of brown tides caused by *Sargassum* spp. on near-shore Caribbean seagrass communities. Mar. Pollut. Bull. 122, 272–281.
van Tussenbroek, B.I., Monroy-Velázquez, L.V., García-Sánchez, M., Ruiz-Fernández, A. C., Valencia-Castañeda, G., Paéz-Osuna, F., Arenas, P., Rojas-González, R.I.,

Gracia, A., 2024a. Biochemistry and associated fauna of holopelagic *Sargassum* spp. in the Caribbean Sea. Mar. Biol. 171.
van Tussenbroek, B.I., Monroy-Velázquez, L.V., Rodríguez, D., Suescún-Bolívar, L.P., Thomé, P.E., Cerqueda-García, D., García-Maldonado, J.Q., Martínez-López, I.G., López-Portillo, J.A., Barba-Santos, M.G., Gomez-Reali, M.A., Escalante-Mancera, J. E., 2024b. Monitoring drift and associated biodiversity of nearshore rafts of holopelagic *Sargassum* spp. in the Mexican Caribbean. Aquat. Bot. 195.
Wang, R.J., Xiao, H., Zhang, P.Y., Qu, L., Cai, H.J., Tang, X.X., 2007. Allelopathic effects of *Ulva pertusa*, *Corallina pilulifera* and *Sargassum thunbergii* on the growth of the dinoflagellates *Heterosigma akashiwo* and *Alexandrium tamarense*. J. Appl. Phycol. 19, 109–121.
Wang, Y., Zhou, B., Tang, X.X., 2009. Effects of two species of macroalgae-*Ulva pertusa* and *Gracilaria lemaneiformis*-on growth of *Heterosigma akashiwo* (Raphidophyceae). J. Appl. Phycol. 21, 375–385.
Wang, R.J., Feng, L., Tang, X.X., Wang, J.H., Dung, S.L., 2012. Allelopathic growth inhibition of *Heterosigma akashiwo* by the three *Ulva* species (*Ulva Pertusa*, *Ulva linza*, *Enteromorpha intestinalis*) under laboratory conditions. Acta Oceanol. Sin. 31, 138–144.
Wang, M.Q., Hu, C.M., Barnes, B.B., Mitchum, G., Lapointe, B., Montoya, J.P., 2019. The great Atlantic *Sargassum* belt. Science 365, 83–+.
Webb, W.L., Newton, M., Starr, D., 1974. Carbon-dioxide exchange of *Alnus rubra* : A mathematical model. Oecologia 17, 281–291.
Zhang, Y.R., Xu, N.J., Li, Y.H., 2021. Effect of the extracts of *Sargassum fusiforme* on red tide microalgae in East China Sea. Front. Mar. Sci. 8, 628295.
Zhu, Y., Ishizaka, J., Tripathy, S., Wang, S., Mino, Y., Matsuno, T., Suggett, D.J., 2016. Variation of the photosynthetic electron transfer rate and electron requirement for daily net carbon fixation in Ariake Bay, Japan. J. Oceanogr. 72, 761–776.